Interlayer excitons in $MoSe_2/WSe_2$ heterostructures from first principles

Roland Gillen[1,2,*] and Janina Maultzsch[2]

[1]*Institute of Solid State Physics, TU Berlin, Hardenbergstrasse 36, 10623 Berlin, Germany*

[2]*Department of Physics, Friedrich-Alexander University Erlangen-Nürnberg, Staudtstrasse 7, 91058 Erlangen, Germany*

(Received 26 December 2017; revised manuscript received 6 April 2018; published 16 April 2018)

Based on *ab initio* theoretical calculations of the optical spectra of vertical heterostructures of $MoSe_2$ (or MoS_2) and WSe_2 sheets, we reveal two spin-orbit-split Rydberg series of excitonic states below the A excitons of $MoSe_2$ and WSe_2 with a significant binding energy on the order of 250 meV for the first excitons in the series. At the same time, we predict from accurate many-body G_0W_0 calculations that crystallographically aligned $MoSe_2/WSe_2$ heterostructures exhibit an indirect fundamental band gap. Due to the type-II nature of the $MoSe_2/WSe_2$ heterostructure, the indirect transition and the exciton Rydberg series corresponding to a direct transition exhibit a distinct interlayer nature with spatial charge separation of the coupled electrons and holes. Our calculations confirm the recent experimental observation of a doublet nature of the long-lived states in photoluminescence spectra of MoX_2/WY_2 heterostructures, and we attribute these two contributions to momentum-direct interlayer excitons at the K point of the hexagonal Brillouin zone and to momentum-indirect excitons at the indirect fundamental band gap. Our calculations further suggest a noticeable effect of stacking order on the electronic band gaps and on the peak energies of the interlayer excitons and their oscillation strengths.

DOI: 10.1103/PhysRevB.97.165306

I. INTRODUCTION

Transition-metal dichalcogenides (TMDCs) of molybdenum and tungsten are promising members of the family of layered materials due to the versatility of their physical properties. On one hand, they are intrinsic semiconductors in bulk and few-layer phases, with a direct fundamental band gap in the monolayer form. This band-gap transition, accompanied by strong excitonic effects, leads to an enhancement of photoluminescence quantum yield for decreasing material thickness [1–6]. It inspired applications of TMDCs in novel thin and flexible optoelectronic devices, such as photodiodes [7,8], photodetectors [9], or single-photon emitters [10–13]. On the other hand, the heavy transition-metal atoms possess a significant spin-orbit interaction that causes a split of the valence band edge. The associated coupled spin and valley physics open a path towards a combination of spin- and valleytronics [14,15].

An additional advantage of layered materials such as TMDCs is the saturated covalent bonds within one layer and noncovalent binding between the layers, which allows for atomically sharp and stress-free interfaces between two different layered materials, e.g., in $p-n$ junctions made of $MoSe_2$ and WSe_2 [16] or similar materials. Heterostructures of transition-metal dichalchogenides with other materials thus offer a powerful path to engineer flexible compound materials and devices with desired optical and electronic properties. The vertical or lateral combination of sheets of Mo and W TMDCs recently gained particular interest due to the observation of long-lived excitonic states in the photoluminescence spectra of MoS_2/WS_2 [17], MoS_2/WSe_2 [18,19], $MoSe_2/WSe_2$ [20–23], and $MoSe_2/WS_2$ [24] heterostructures. Due to the expected type-II alignment [25] of MoX_2 and WX_2 bands (with $X = S$, Se, Te), this observation has been attributed to interlayer excitons with a spatial separation of the coupled electrons and holes, which is of interest for applications in photovoltaics.

Despite this interest, theoretical confirmations of this interpretation from *ab initio* are scarce and indirect so far [26–28]. Another recent study [29] employed a generalized Mott-Wannier model to vertical $MoS_2/BN/WSe_2$ heterostructures, which is limited to the exciton binding energy. This lack of studies in the literature can be understood from the complications of *ab initio* simulations of the excitonic spectra in two-dimensional (2D) TMDC heterostructures due to the lowered symmetry, the necessity of careful treatment of the quasi-two-dimensional dielectric screening, and the importance of strong spin-orbit coupling for both the band alignment in stacked heterostructures and the nature of excitonic transitions.

We thus report fully *ab initio* theoretical simulations of the optical spectra of $MoSe_2/WSe_2$ and MoS_2/WSe_2 heterostructures under full inclusion of electron-hole and spin-orbit interactions. Our computations allow a direct estimate of the expected exciton binding energy and give access to the excitonic wave functions. By considering three distinct stacking orders, we assess the possible influence of arbitrary alignment of the layers in experimental conditions.

II. METHOD

We calculated the ground-state electronic wave functions and band structures with the QUANTUM ESPRESSO package [30] in the Perdew-Burke-Ernzerhof (PBE) approximation, using fully relativistic normconserving pseudopotentials [31] including the semicore s and p orbitals of Mo and W. Atomic positions and cell parameters were relaxed with inclusion of semiempirical van der Waals corrections from the PBE+D3 [32] scheme.

*roland.gillen@fau.de

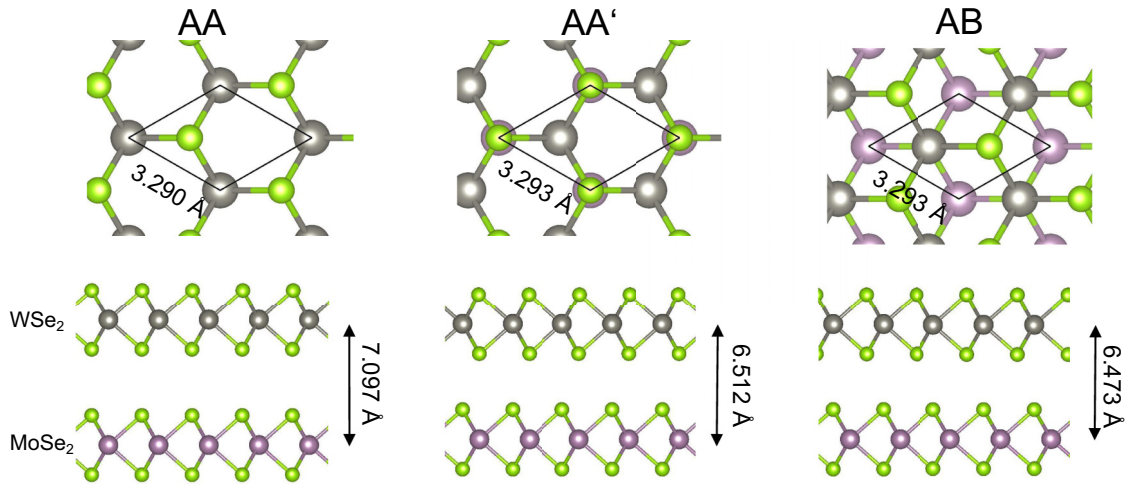

FIG. 1. Geometries of the computed heterostructures of monolayers of $MoSe_2$ and WSe_2 with AA, AA', and AB stackings. Indicated are the optimized in-plane lattice constants and layer distances. The typical stacking in bilayer and bulk MoS_2, $MoSe_2$, and WSe_2 corresponds to AA'.

The dielectric functions including electron-hole interactions and spin-orbit interactions were computed by solving the Bethe-Salpeter equation (BSE) using the YAMBO code [33] on a discrete grid of $21\times21\times1$ k points. Twenty valence bands and 20 conduction bands were included for the calculation of the absorption spectra. The static dielectric function was calculated with 600 empty bands and a cutoff for the response function of 200 eV. The electronic band structures from density functional theory (DFT) were corrected by G_0W_0 quasiparticle energies using 1500 unoccupied bands. The exchange and correlation contributions were extrapolated to an infinite cutoff energy [34]. In both GW and BSE calculations, we used the effective energy technique [35] to include contributions from high-energy unoccupied bands.

We found it crucial for quasi-two-dimensional materials to properly treat the singularity of the Coulomb interaction in order to obtain interpretable quantitative results. We truncated the Coulomb interaction in the nonperiodic direction following the method from Ref. [36] and averaged the head of the screened Coulomb interaction W, i.e., the contribution $W(\mathbf{q}\rightarrow\mathbf{0}, \mathbf{G}\rightarrow\mathbf{0},\mathbf{G}'\rightarrow\mathbf{0})$ by using a model function for the dielectric screening in the vicinity of the Γ point. Our results suggest that different treatments of the Coulomb interaction [36–39] and the dielectric screening [40,41] close to the Γ point account for some of the spread in the calculated excitonic binding energies in TMDCs found in the literature. We refer to the Supplemental Material [42] for further computational details.

III. RESULTS AND DISCUSSION

Experimental samples of vertical heterostructures are often fabricated from exfoliation procedures, where individual layers are stacked manually, typically exhibiting an arbitrary stacking order. The local layer alignment can affect the electronic band structure of the composite material through the formation of interface dipoles (adding a relative shift of the band structures of the two materials) and interlayer hybridization of orbitals. The latter should be particularly strong at Γ and similar points in the Brillouin zone that possess considerable contributions from chalcogen p states, as has been shown for mixed heterostructures [43] and twisted bilayers of the same material [44].

In order to obtain an estimate of the effects of relative alignment on the electronic band structures and simulated optical spectra of $MoSe_2$-WSe_2, we consider three different stacking orders that all have the advantage of preserving the hexagonal symmetry of the pure materials: The AA stacking corresponds to a zero degree rotation of the WSe_2 with respect to the $MoSe_2$ layer. AA' is the most stable stacking in $MoSe_2$ and WSe_2 bilayer and bulk with a 180° relative rotation. The AB stacking is an AA stacking with a relative shift between $MoSe_2$ and WSe_2 layers by $a/\sqrt{3}$, where a is the in-plane lattice constant, and the preferred stacking of rhombohedral ($3R$-) MoS_2, graphite, and hexagonal boron nitride.

Figure 1 shows the optimized geometries obtained from our PBE-D3 calculations. The different stackings have only a minor effect on the in-plane lattice constants, with a variation of about 0.1%. The obtained lattice constants of 3.290–3.293 Å are only slightly changed compared to the monolayer materials and are in good agreement with the experimental lattice constants of bulk $MoSe_2$ and WSe_2 of 3.28–3.29 Å [45]. On the other hand, the interlayer distance shows a significantly stronger variation. For AA stacking, the chalcogen atoms of the two layers are right on top of each other, which leads to an increased interlayer distance of about 7.1 Å. For the other stackings, the chalcogen atoms are aligned with the metal atoms of the neighboring layer (AA') or are partially aligned with the centers of the neighboring metal-selenium hexagons. The resulting interlayer distances of 6.51 Å (AA') and 6.47 Å (AB) are only slightly larger than the interlayer distances in AA' stacked bilayer $MoSe_2$ and WSe_2. We used these optimized geometries to calculate the electronic band structures of the three heterostructures, shown in Fig. 2. A full spin-orbit interaction was included to correctly describe the large spin-orbit splitting of the valence and conduction bands at the K point in the hexagonal Brillouin zone. The bands at the K point show only negligible signs of hybridization for the three stacking orders, due to the dominant contributions from Mo and W d states. In accordance with previous studies

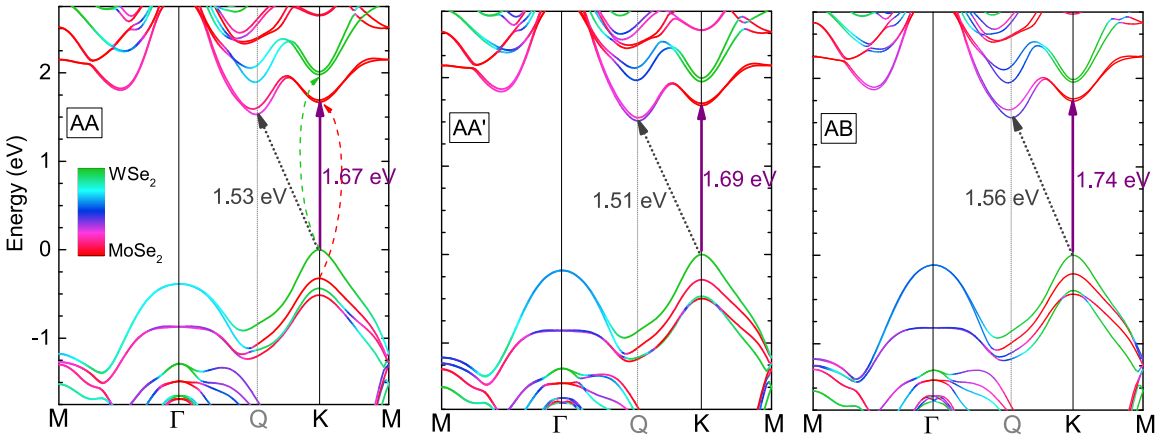

FIG. 2. Electronic band structures for three different stackings of monolayers of $MoSe_2$ and WSe_2. All computations were corrected by G_0W_0 quasiparticle energies and by full inclusion of spin-orbit interactions. The zero of energy is set to the valence band maximum for each stacking. The color scale depicts the relative contributions of the materials to the bands.

[25], the bands of $MoSe_2$ and WSe_2 are shifted relative to each other such that the global valence band maximum is in the WSe_2 layer (green color in Fig. 2) and the conduction band valley is in the $MoSe_2$ layer (shown in red). The stacking order affects the band alignment and the size of the direct interlayer band gap at K, as shown in Fig. 3. We compiled the band offsets for the three stacking orders in Table I.

On the other hand, the main qualitative differences of the electronic band structures due to different layer stackings are found at the valence band edge at the Γ point and the conduction band valley around the halfway point (Q) in the Γ-K direction. At the Γ point, the bands of the two materials are prone to hybridization due to contributions from Se p states, causing split bands of mixed $MoSe_2$ and WSe_2 character. Interestingly, the interlayer interaction in all three stacking orders appears to be strong enough to pull down the conduction band valley at the Q point, similar to the case of homobilayers of $MoSe_2$ and WSe_2. This shifts the global conduction band minimum from the K point to the Q point. The second lowest conduction band at the Q valley is dominated by Mo $d_{x^2-y^2}$ and Se p_x/p_y states of the $MoSe_2$ layer, while the lowest conduction band obtains larger contributions from the WSe_2 layer for decreasing interlayer distance but mainly remains within the $MoSe_2$ layer. Our simulations thus suggest that $MoSe_2$ and WSe_2, especially for random stacking configurations, form a type-II heterostructure with an *indirect* fundamental band gap [46]. This introduces the possibility of momentum-indirect excitons with a strong interlayer nature as candidates for the experimentally observed interlayer excitons.

We will now show that, in addition to the indirect transition discussed above, a second interlayer transition at the K and K' points leads to strong excitonic effects and can be attributed to the experimentally observed interlayer transition. Based on the electronic structures in Fig. 2, we used the excitonic Bethe-Salpeter equation (BSE) to compute the corresponding absorption spectra from direct band transitions [47] including electron-hole effects for the three stacking orders. An advantage of this theoretical approach is the ability to decompose the obtained spectra into the contributing band transitions. As shown in Fig. 4, for AA, AA', and AB stacking, the absorption onset is dominated by a number of excitonic contributions with high oscillator strengths. The lowest-energy bright contribution W_A originates from a transition between the valence band top and the fourth conduction band at the K point and corresponds to the A exciton in isolated single-layer WSe_2. In Fig. 5(a) we show the excitonic wave function of W_A. Both the electron and hole parts of the excitonic wave function are localized within the WSe_2 layer. Similarly, the contribution Mo_A corresponds to the A exciton of single-layer $MoSe_2$ and appears at a slightly higher energy due to the difference in spin-orbit splitting of the valence band top for $MoSe_2$ and WSe_2. The excitonic wave function of Mo_A [Fig. 5(b)] is localized within the $MoSe_2$ layer.

The computational expense of BSE calculations including spin-orbit coupling limited us to a grid of 21×21 k points for the Brillouin zone integration, which might be insufficient to yield fully converged values for the exciton binding energies. As the spin-orbit interaction only affects the absolute energy of the A excitons but not the binding energy, we hence performed

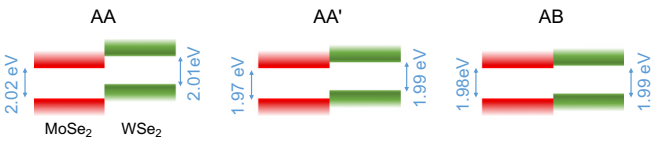

FIG. 3. Schematic band alignment for the three studied stacking orders with intralayer band gaps at the K point. The band-gap value energies given are taken from the calculations shown in Fig. 2.

TABLE I. Band offsets obtained from G_0W_0 calculations. For the conduction band, we give the band offsets between $MoSe_2$ and WSe_2 dominated bands at the Q and the K points.

	Stacking order		
Band offsets	AA	AA'	AB
ΔE_V (meV)	326	284	209
ΔE_C^K (meV)	313	270	216
ΔE_C^Q (meV)	362	458	394

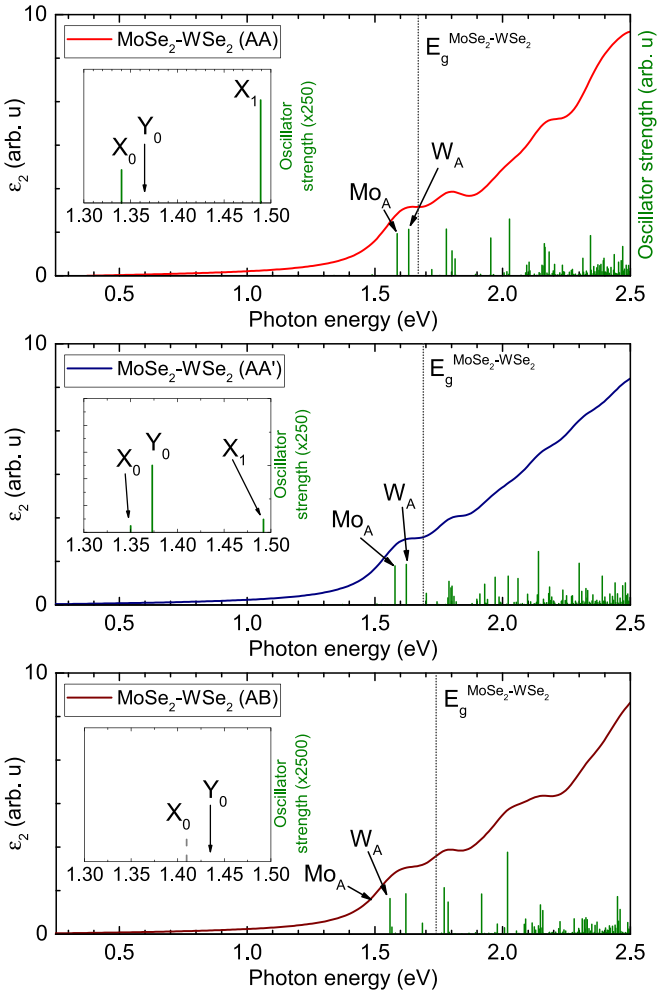

FIG. 4. Calculated dielectric functions ϵ_2 for three stackings with electron-hole effects and spin-orbit coupling and light polarization *parallel* to the layer plane of the heterostructure. Green bars show the optical oscillator strengths of the constituting excitonic and band transitions. The insets show the energy region around the zero-order interlayer excitonic peaks. The dashed line in the inset for AB stacking shows the X_0 transition for light polarization *perpendicular* to the surface. The intensity for light polarized parallel to the plane vanishes. Note the different scale in the inset for AB stacking.

additional calculations without spin-orbit coupling but with denser 33×33 k-point grids. For AA' stacking, we derive exciton binding energies of 267 and 307 meV for W_A and Mo_A, respectively, with similar results for the AA and AB stacking orders. The exciton binding energies are reduced as compared to the isolated single-layer materials (0.48 eV for $MoSe_2$ [48], 0.46 eV for WSe_2), due to dielectric screening from the neighboring layer in the heterostructure. We will now show that these transitions can be identified with the *interlayer* excitons as proposed from experiments.

In addition to the excitonic contributions from *intralayer* transitions discussed above, our calculations reveal further contributions with low oscillator strengths at energies below the A excitons. These contributions form two Rydberg-like series of electronic transitions at the fundamental band gap (labeled X_n in the insets to Fig. 4) and between the valence band maximum and the second conduction band (Y_n). The energy of the "ground state" (i.e., $n = 0$) contributions is well below the energy of the fundamental band transition, indicating an excitonic state, and is relatively independent of the stacking order in the heterostructure. As the involved valence band maximum and conduction band minimum are composed of WSe_2 and $MoSe_2$ states, respectively, we attribute X_n and Y_n to *interlayer* excitons with a distinct charge separation. This charge separation is clearly seen in the plot of the exciton wave function of Y_0 (for AA' stacking) in Fig. 5(c): The electronic part of the exciton wave function is confined to the $MoSe_2$ layer, while the hole contribution is confined to the WSe_2 layer. We note that due to the 180° relative rotation of the layers in the AA' stacking, the K point of the $MoSe_2$ layer is rotated onto the K' point of the WSe_2 layer (and vice versa). Due to the swapped order of the spin-orbit-split bands at K' compared to the K point, the Y_0 transition in AA' stacking hence corresponds to the X_0 peak for the AA and AB stackings.

The difference in fundamental band gaps induces small relative shifts of the transition energies of X_0 and Y_0 for the three different stackings (see Fig. 4). Using a denser grid of 33×33 k points and neglecting the spin-orbit interaction, we estimate the binding energy of X_0 and Y_0 to be on the order of 250 meV for the three different stacking orders, which is of a similar magnitude as the value of 280 meV derived from a Mott-Wannier model for a vertical MoS_2/WSe_2 heterostructure [29]. The different stacking orders induce a small variation of 10 meV between the highest (AB stacking) and lowest (AA stacking) binding energy. The obtained peak energies and the energies compared to the corresponding electronic band gaps are summarized for the AA' stacking order in Table II. Surprisingly, the binding energies of X_0 and Y_0 excitons are very similar to the binding energies of the intralayer excitons, as discussed above. This appears counterintuitive due to the spatial separation of electrons and holes for the interlayer excitons. On the other hand, the spatial extension of the excitonic wave functions within the layers is on the order of several nm and hence significantly larger than the distance of the two layers, and the dielectric screening in the heterostructure is anisotropic. It is thus possible that the influence of the spatial separation on the electron-hole interaction is compensated by a reduction of the Coulomb screening in the interstitial region between the $MoSe_2$ and WSe_2 layers.

While the peak and exciton binding energies of the spatially indirect (and momentum-direct) excitons show a relatively weak dependence on the stacking order, the oscillator strengths vary quite significantly. In particular, they almost completely vanish for AB stacking in case of light polarized parallel to the plane of the 2D heterostructure. Interestingly, the X_0 transition is "activated" for light polarized *perpendicular* to the surface [refer to the inset of Fig. 4(c)]. Similarly, a number of nominally spin-forbidden transitions gain oscillation strength under these conditions. This motivates a more detailed study of the optical selection rules and spinorial symmetries for different stacking orders. The found strong dependence of oscillator strength on stacking order might be one of the reasons for the experimental perception that interlayer excitons cannot be always detected.

In order to better understand the origin of these observations, we used the WANNIER90 code [49] to project the matrix

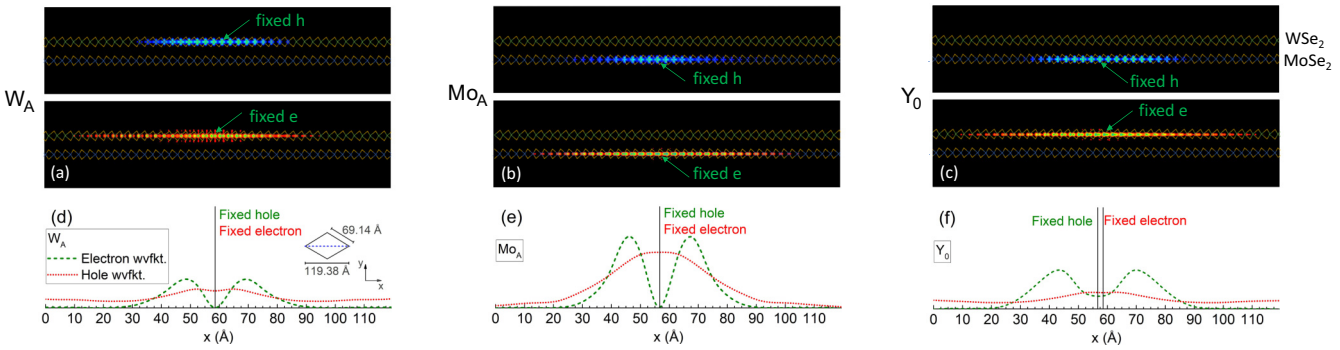

FIG. 5. Electron (blue) and hole (red) contributions to the excitonic wave functions of the (a) W_A, (b) Mo_A, and (c) X_0 excitons of an AA'-stacked $MoSe_2/WSe_2$ heterostructure. The atomic structure of the two layers is indicated in each panel: The upper layer is WSe_2 and the lower layer is $MoSe_2$. The excitonic wave functions were computed for a supercell of 21×21 unit cells and projected onto the $x-z$ plane. For the electron (e) [hole (h)] contributions, the hole (electron) was fixed at the Mo (W), atom indicated by the green arrows. (d)–(f) Envelope functions of the electron and hole parts of the excitonic wave functions from (a)–(c) along a path in the x direction depicted as a dashed line in the inset in (d). The path was chosen to contain the fixed electron/hole. The shape of the electronic part of the excitonic wave functions agrees with Ref. [37]. Top views of the excitonic wave functions and a discussion of the spatial extension of the electron and hole parts can be found in the Supplemental Material [42].

elements for interlayer transitions at K (neglecting electron-hole interaction effects) to a basis of atomic orbitals. Based on our calculations, it is reasonable to assume that the different polarization behaviors arise from weak interlayer hybridization at the K point that causes a small, stacking-dependent, mixing of Mo d states into the valence band maximum (see Fig. 6). Our calculations suggest that the optical matrix elements are dominated by transitions between the spilled-over Mo d states with the conduction band minimum. This would explain the generally observed much lower oscillation strengths of the X_0 and Y_0 compared to the intralayer Mo_A and W_A transitions, which are in agreement with recent photocurrent measurements on $MoSe_2/WSe_2$ heterostructures [21], and should apply similarly for spatially indirect transitions at the indirect fundamental band gap of the system. It would also explain why the polarization dependence of X_0 is different from that of Mo_A and W_A for AB stacking. We found a similar Rydberg series of interlayer excitonic states with low oscillation strengths for a MoS_2/WSe_2 bilayer heterostructure as well. We refer to the Supplemental Material [42] for calculated absorption spectra for light polarization perpendicular to the heterostructure slab, details about the projection of the optical matrix elements, and for the calculations on the MoS_2/WSe_2 bilayer heterostructure.

The very small oscillator strengths suggest that the interlayer excitons are not visible in absorption measurements.

TABLE II. Peak positions (E) and binding energies (E_b) of selected excitonic transitions with respect to the corresponding electronic band gaps (E_g) for AA' stacking. For the binding energy, we give two different values for calculations with (E_b^{SOI}) and without ($E_b^{\mathrm{no\ SOI}}$) spin-orbit coupling. The X_0 transition occurs between the highest valence band (in the WSe_2 layer) and the lowest conduction band (in the $MoSe_2$ layer) at the K point, while the Y_0 transition occurs between the highest valence and the second lowest conduction band. The converged exciton binding energies are shown in bold.

		21×21 k-point grid		33×33 grid
Excitation	E_g (eV)	E (eV)	E_b^{SOI} (eV)[a]	$E_b^{\mathrm{no\ SOI}}$ (eV)[b]
Mo_A	1.978	1.578	0.41	**0.307**
Mo_A^*		1.701	0.277	**0.176**
Mo_A^{**}		1.733	0.245	**0.131**
W_A	1.994	1.623	0.377	**0.267**
W_A^*		1.791	0.203	**0.156**
W_A^{**}		1.835	0.159	**0.121**
Mo_B	2.22	1.80	0.42	
W_B	2.432	2.06	0.372	
X_0	1.685	1.350	0.335	**0.251**
X_1	($K\rightarrow K$)	1.492	0.193	**0.148**
Y_0	1.709	1.373	0.336	
Y_1	($K\rightarrow K$)	1.509	0.200	
Indirect band gap	1.51 ($K\rightarrow Q$)			

[a]Obtained with a 21×21 k-point sampling. Due to the spatial extent of the excitonic wave functions, the binding energies are overestimated for this sampling.

[b]Obtained with a $33\times33\times1$ k-point sampling that yields accurate exciton binding energies. Inclusion of spin-orbit coupling has negligible effects on the results.

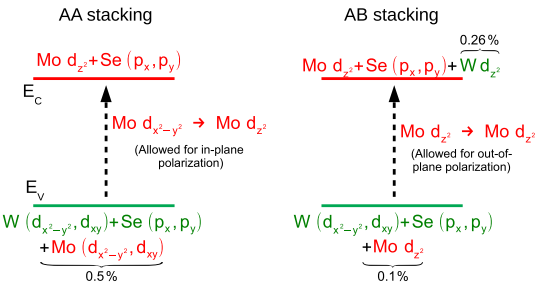

FIG. 6. Schematic composition of the band edges E_V and E_C at the K point for AA and AB stacking. Small stacking-dependent mixing of states of the neighboring layer occurs due to weak interlayer hybridization. For each stacking order, the main contribution to the optical oscillator strength of interlayer transitions is shown by a dashed arrow.

On the other hand, they might be visible as excitonic states in photoluminescence (PL) measurements due to a radiative recombination of electron-hole pairs that have relaxed to the band extrema. In this context, our calculations suggest two possible contributions to the experimentally observed interlayer exciton: (i) spatially indirect, momentum-direct recombinations of the X_0 and Y_0 excitons at the K point with a substantial binding energy of 250 meV, and (ii) a spatially indirect, momentum-indirect recombination at the indirect fundamental band gap. Based on a comparison of our calculated indirect band gap of 1.5 eV with the position of the interlayer PL peak, we estimate the exciton binding energy to be of order 0.1–0.2 eV. This estimate appears reasonable in light of the significant binding energy of the momentum-direct interlayer excitons at the K point and is further supported by the good prediction of the electronic band gaps and peak positions of the intralayer A excitons compared to experiments. The first contribution might be enabled by inefficient relaxation of excited electrons from the K to the Q conduction band valley, similar to the observations from photoluminescence experiments on homobilayers of $MoSe_2$ and WSe_2, where the $MoSe_2$ and WSe_2 A peak appears together with the indirect transition.

On the other hand, from a naive point of view, the efficiency of the first pathway should be limited by its twofold indirect nature. Our results are in good qualitative and quantitative agreement with the recent photoluminescence experiments by Miller *et al.* [23], who showed the observed interlayer peak to consist of two contributions with different temperature behaviors. Our calculations confirm their interpretation that the emission arises from two different kinds of interlayer excitations, one direct in momentum space [(ii)] and one indirect in momentum space [(i)]. This raises the question of the detailed nature of the intralayer scattering that assists the momentum-indirect emission. Our calculations suggest a difference between the fundamental indirect and direct band gaps on the order of 140 meV, significantly larger than the highest phonon energy in monolayer $MoSe_2$ of about 45 meV [50]. Further insights into the relative strength and dynamics of both contributions to the interlayer exciton signal may be revealed by further time-resolved optical experiments and explicit *ab initio* calculations of momentum-indirect excitons with the inclusion of electron-phonon interaction effects in these heterostructures.

IV. CONCLUSION

To conclude, we predict that mixed MoX_2/WY_2 vertical heterostructures host two spin-orbit-split Rydberg series of excitonic transitions at the K point with spatial confinement of the electron and hole parts to the MoX_2 and WSe_2 layers, respectively. Their binding energy is around 250 meV for the lowest-energy interlayer exciton. Our calculations suggest that the $MoSe_2/WSe_2$ heterostructure exhibits a fundamental band gap which is indirect in reciprocal space *and* in real space. Taking into account the exciton binding energies, we find a second optical transition at a similar energy, which is direct in reciprocal space (at the K and K' points of the Brillouin zone) but still indirect in real space. Such interlayer transitions (i.e., spatially indirect) are attributed to the interlayer transitions to experimentally observed additional photoluminescence peaks and explain the asymmetric shape of the photoluminescence peaks that was recently reported to stem from a doublet of two unequal contributions. Low oscillation strengths cause these interlayer excitons to be undetectable in absorption experiments. Our calculations show that different band alignments and orbital overlaps between the constituent layers in different stacking orders have a relatively weak effect on the peak energies of the interlayer excitons but a significant effect on the oscillation strengths and their (linear) polarization dependence. The spatial separation of electrons and holes in the energetically lowest excited state makes such heterojunctions interesting for use in thin and flexible photovoltaic devices.

Note added. Recently, we became aware of two additional reports [51,52] with theoretical calculations for MoS_2/WS_2 heterostructures. The results are compatible with our work. Further, we also became aware of an article on $MoSe_2/WSe_2$ heterostructures with results similar to ours [53].

ACKNOWLEDGMENTS

Computational resources used for the simulations in this work were provided by the North-German Supercomputing Alliance (HLRN) under Project No. bep00047. The authors acknowledge financial support by the Deutsche Forschungsgemeinschaft (DFG) within the Cluster of Excellence "Engineering of Advanced Materials" (Project No. EXC 315) (Bridge Funding).

[1] K. F. Mak, C. Lee, J. Hone, J. Shan, and T. F. Heinz, Phys. Rev. Lett. **105**, 136805 (2010).

[2] A. Splendiani, L. Sun, Y. Zhang, T. Li, J. Kim, C.-Y. Chim, G. Galli, and F. Wang, Nano Lett. **10**, 1271 (2010).

[3] S. Tongay, J. Suh, C. Ataca, W. Fan, A. Luce, J. S. Kang, J. Liu, C. Ko, R. Raghunathanan, J. Zhou, F. Ogletree, J. Li, J. C. Grossman, and J. Wu, Sci. Rep. **3**, 2657 (2013).

[4] H. R. Gutierrez, N. Perea-Lopez, A. L. Elías, A. Berkdemir, B. Wang, R. Lv, F. Lopez-Urias, V. H. Crespi, H. Terrones, and M. Terrones, Nano Lett. **13**, 3447 (2012).

[5] S. Mouri, Y. Miyauchi, and K. Matsuda, Nano Lett. **13**, 5944 (2013).

[6] N. Scheuschner, O. Ochedowski, A.-M. Kaulitz, R. Gillen, M. Schleberger, and J. Maultzsch, Phys. Rev. B **89**, 125406 (2014).

[7] S. Lin, X. Li, P. Wang, Z. Xu, S. Zhang, H. Zhong, Z. Wu, W. Xu, and H. Chen, Sci. Rep. **5**, 15103 (2015).

[8] F. Withers, O. D. Pozo-Zamudio, A. Mishchenko, A. P. Rooney, A. Gholinia, K. Watanabe, T. Taniguchi, S. J. Haigh, A. K. Geim, A. I. Tartakovskii, and K. S. Novoselov, Nat. Mater. **14**, 301 (2015).

[9] O. Lopez-Sanchez, D. Lembke, M. Kayci, A. Radenovic, and A. Kis, Nat. Nanotechnol. **8**, 497 (2013).

[10] P. Tonndorf, R. Schmidt, R. Schneider, J. Kern, M. Buscema, G. A. Steele, A. Castellanos-Gomez, H. S. J. van der Zant, S. M. de Vasconcellos, and R. Bratschitsch, Optica **2**, 347 (2015).

[11] Y.-M. He, G. Clark, J. R. Schaibley, Y. He, M.-C. Chen, Y.-J. Wei, X. Ding, Q. Zhang, W. Yao, X. Xu, C.-Y. Lu, and J.-W. Pan, Nat. Nanotechnol. **10**, 497 (2015).

[12] C. Chakraborty, L. Kinnischtzke, K. M. Goodfellow, R. Beams, and A. N. Vamivakas, Nat. Nanotechnol. **10**, 507 (2015).

[13] A. Srivastava, M. Sidler, A. V. Allain, D. S. Lembke, A. Kis, and A. Imamoğlu, Nat. Nanotechnol. **10**, 491 (2015).

[14] D. Xiao, G.-B. Liu, W. Feng, X. Xu, and W. Yao, Phys. Rev. Lett. **108**, 196802 (2012).

[15] O. L. Sanchez, D. Ovchinnikov, S. Misra, A. Allain, and A. Kis, Nano Lett. **16**, 5792 (2016).

[16] N. Flöry, A. Jain, P. Bharadwaj, M. Parzefall, T. Taniguchi, K. Watanabe, and L. Novotny, Appl. Phys. Lett. **107**, 123106 (2015).

[17] Y. Yu, S. Hu, L. Su, L. Huang, Y. Liu, Z. Jin, A. A. Purezky, D. B. Geohegan, K. W. Kim, Y. Zhang, and L. Cao, Nano Lett. **15**, 486 (2015).

[18] H. Fang, C. Battaglia, C. Carraro, S. Nemsak, B. Ozdol, J. S. Kang, H. A. Bechtel, S. B. Desai, F. Kronast, A. A. Unal, G. Conti, C. Conlon, G. K. Palsson, M. C. Martin, A. M. Minor, C. S. Fadley, E. Yablonovitch, R. Maboudian, and A. Javey, Proc. Natl. Acad. Sci. USA **111**, 6198 (2014).

[19] R. Cheng, D. Li, H. Zhou, C. Wang, A. Yin, S. Jiang, Y. Liu, Y. Chen, Y. Huang, and X. Duan, Nano Lett. **14**, 5590 (2014).

[20] P. Rivera, J. R. Schaibley, A. M. Jones, J. S. Ross, S. Wu, G. Aivazian, P. Klement, K. Seyler, G. Clark, N. J. Ghimire, J. Yan, D. G. Mandrus, W. Yao, and X. Xu, Nat. Commun. **6**, 6242 (2015).

[21] J. S. Ross, P. Rivera, J. Schaibley, E. Lee-Wong, H. Yu, T. Taniguchi, K. Watanabe, J. Yan, D. Mandrus, D. Cobden, W. Yao, and X. Xu, Nano Lett. **17**, 638 (2017).

[22] P. K. Nayak, Y. Horbatenko, S. Ahn, G. Kim, J.-U. Lee, K. Y. Ma, A.-R. Jang, H. Lim, D. Kim, S. Ryu, H. Cheong, N. Park, and H. S. Shin, ACS Nano **11**, 4041 (2017).

[23] B. Miller, A. Steinhoff, B. Pano, J. Klein, F. Janke, A. Holleitner, and U. Wurstbauer, Nano Lett. **17**, 5229 (2017).

[24] D. Kozawa, A. Carvalho, I. Verzhbitskiy, F. Giustiniano, Y. Miyauchi, S. Mouri, A. H. C. Neto, K. Matsuda, and G. Eda, Nano Lett. **16**, 4087 (2016).

[25] J. Kang, S. Tongay, J. Zhou, J. Li, and J. Wu, Appl. Phys. Lett. **102**, 012111 (2013).

[26] H.-P. Komsa and A. V. Krasheninnikov, Phys. Rev. B **88**, 085318 (2013).

[27] M. Palummo, M. Bernardi, and J. C. Grossman, Nano Lett. **15**, 2794 (2015).

[28] S. Gao, L. Yang, and C. D. Spataru, Nano Lett. **17**, 7809 (2017).

[29] S. Latini, K. T. Winther, T. Olsen, and K. S. Thygesen, Nano Lett. **17**, 938 (2017).

[30] P. Giannozzi, S. Baroni, N. Bonini, M. Calandra, R. Car, C. Cavazzoni, D. Ceresoli, G. L. Chiarotti, M. Cococcioni, I. Dabo, A. D. Corso, S. de Gironcoli, S. Fabris, G. Fratesi, R. Gebauer, U. Gerstmann, C. Gougoussis, A. Kokalj, M. Lazzeri, L. Martin-Samos *et al.*, J. Phys.: Condens. Matter **21**, 395502 (2009).

[31] M. Schlipf and F. Gygi, Comput. Phys. Commun. **196**, 36 (2015).

[32] S. Grimme, S. Ehrlich, and K. Goerigk, J. Comput. Chem. **32**, 1456 (2011).

[33] A. Marini, C. Hogan, M. Grüning, and D. Varsano, Comput. Phys. Commun. **180**, 1392 (2009).

[34] J. Klimeš, M. Kaltak, and G. Kresse, Phys. Rev. B **90**, 075125 (2014).

[35] F. Bruneval and X. Gonze, Phys. Rev. B **78**, 085125 (2008).

[36] S. Ismail-Beigi, Phys. Rev. B **73**, 233103 (2006).

[37] A. Molina-Sánchez, D. Sangalli, K. Hummer, A. Marini, and L. Wirtz, Phys. Rev. B **88**, 045412 (2013).

[38] C. A. Rozzi, D. Varsano, A. Marini, E. K. U. Gross, and A. Rubio, Phys. Rev. B **73**, 205119 (2006).

[39] F. A. Rasmussen, P. S. Schmidt, K. T. Winther, and K. S. Thygesen, Phys. Rev. B **94**, 155406 (2016).

[40] F. Hüser, T. Olsen, and K. S. Thygesen, Phys. Rev. B **88**, 245309 (2013).

[41] D. Y. Qiu, F. H. da Jornada, and S. G. Louie, Phys. Rev. B **93**, 235435 (2016).

[42] See Supplemental Material at http://link.aps.org/supplemental/10.1103/PhysRevB.97.165306 for a more detailed explanation of the computational approach, top views of the inter- and intralayer excitonic wave functions, plots of the calculated absorption spectra for light polarization perpendicular to the heterostructure slab, a discussion of the optical matrix elements of intra- and interlayer excitons, electronic band structures of $MoSe_2/WSe_2$ for various stackings from the HSE06 hybrid functional, and for calculated absorption spectra of a MoS_2/WSe_2 bilayer heterostructure, which includes Refs. [54–57].

[43] K. Wang, B. Huang, M. Tian, F. Ceballos, M.-W. Lin, M. Mahjouri-Samani, A. Boulesbaa, A. A. Puretzky, C. M. Rouleau, M. Yoon, H. Zhao, K. Xiao, G. Duscher, and D. B. Geohegan, ACS Nano **10**, 6612 (2016).

[44] K. Liu, L. Zhang, T. Cao, C. Jin, D. Qiu, Q. Zhou, A. Zettl, P. Yang, S. G. Louie, and F. Wang, Nat. Commun. **5**, 4966 (2014).

[45] A. A. Al-Hilli and B. L. Evans, J. Cryst. Growth **15**, 93 (1972).

[46] We note here that the relative energy difference of the conduction band minima at K and Q somewhat depends on the method; for instance, the hybrid functional HSE06 predicts a direct fundamental band gap. The corresponding band structures are shown in Sec. 3 of the Supplemental Material.

[47] Inclusion of indirect transitions with a momentum $\mathbf{q}$ are in principle possible but beyond the scope of this work.

[48] R. Gillen and J. Maultzsch, IEEE J. Sel. Top. Quantum Electron. **23**, 219 (2017).

[49] A. A. Mostofi, J. R. Yates, Y.-S. Lee, I. Souza, D. Vanderbilt, and N. Marzari, Comput. Phys. Commun. **178**, 685 (2008).

[50] S. Horzum, H. Sahin, S. Cahangirov, P. Cudazzo, A. Rubio, T. Serin, and F. M. Peeters, Phys. Rev. B **87**, 125415 (2013).

[51] T. Deilmann, Nano Lett. **18**, 1460 (2018).

[52] M. Okada, A. Kutana, Y. Kureishi, Y. Kobayashi, Y. Saito, T. Saito, K. Watanabe, T. Taniguchi, S. Gupta, Y. Miyata, B. I. Yakobson, H. Shinohara, and R. Kitaura, ACS Nano **12**, 2498 (2018).

[53] E. Torun, A. Molina-Sanchez, H. P. C. Miranda, and L. Wirtz, arXiv:1803.05483.

[54] H. Shi, H. Pan, Y.-W. Zhang, and B. I. Yakobson, Phys. Rev. B **87**, 155304 (2013).

[55] X. Wang, J. R. Yates, I. Souza, and D. Vanderbilt, Phys. Rev. B **74**, 195118 (2006).

[56] J. R. Yates, X. Wang, D. Vanderbilt, and I. Souza, Phys. Rev. B **75**, 195121 (2007).

[57] R. Sundararaman and T. A. Arias, Phys. Rev. B **87**, 165122 (2013).